CHAPTER IV

PHOTOEMISSION CALCULATIONS USING KRONIG-PENNEY MODEL

In chapter III, we have discussed the photoemission calculations from the band states (Fermi level) and surface state of free electron solid like aluminium. Since aluminium is weakly bonded metal, we used a free electron initial state wavefunction ψ_i for the band state photoemission. ψ_i was formulated by way of normal matching of wavefunction at the boundary surface of the solid. The photocurrent was then computed by using the electromagnetic field developed by Bagchi and Kar[21].

To incorporate the band structure effects, a model calculation following Kronig and Penney potential was done as a first step. Kronig-Penney model has been used in connection with surface electronic states by several authors[45-48]. It has been seen that some surface related features come out, at least qualitatively, from these calculations. Schaich and Ashcroft[4] have calculated numerically the photoyield by using the modified form of the Kronig-Penney model. Band structure effects was also included in it. They used the wavefunction of Mitchell[39] for free electron gas in a semi-infinite box and considered the photon field vector $\tilde{A}_\omega(z)$ to remain constant.

However the numerical data as obtained by them in the case of potassium is quite realistic. This is evident for the nature of the photocurrent data obtained by them from various planes below the surface. Steslicka[49] had performed a detailed calculations of the surface states using the Kronig-Penney model both for the semi-infinite and the infinite crystal model. Eldib et al[50] had also applied the Kronig-Penney model to one dimensional crystal. He had calculated only the electronic energy bands for mono- and polyatomic crystals and compared his data with the one computed by using the linear combinations of atomic orbital (LCAO) methods.

In this chapter, we shall use the Kronig-Penney model to represent the crystal potential field by a linear array of rectangular well which would later be transformed into a chain of δ- function wells subject to the area of each well remaining constant as shown in Fig. (4.1). By using essentially the electromagnetic field as discussed in chapter-II, we will calculate the photoemission cross-section. The initial state wavefunction is obtained by matching at the surface. The relevant matrix element then can be written as

$$I = \langle \psi_f | H' | \psi_i \rangle = \int_{-\infty}^{\infty} \psi_f^*(z) H' \psi_i(z) dz$$

$$= \int_{-\infty}^{\infty} \psi_f^*(z) \left[\tilde{A}_\omega(z) \frac{d}{dz} + \frac{1}{2} \frac{d}{dz} \tilde{A}_\omega(z) \right] \psi_i(z) dz \qquad (4.1)$$

In Eq. (4.1) above, $\psi_f(z)$ the final state wavefunction, has the same form as given by Eq. (3.13).

To evaluate the initial state wavefunction $\psi_i(z)$, one generally solves the one-dimensional Schrödinger's equation which can be written as

$$\frac{d^2\psi(z)}{dz^2} + k_i^2\psi(z) = -\frac{2m}{\hbar^2} V(z)\psi(z) \qquad (4.2)$$

where $k_i^2=2mE/\hbar^2$ and $V(z)<0$. One can straight away replace the right hand side of Eq. (4.2) by Dirac δ- function and invoke the use of Green function technique as done by Davison and Levine[48] to calculate the electronic energy bands.

$\psi_i(z)$ is calculated[51] by proper matching of ψ and $d\psi/dz$ on the boundary plane defined by z=0 plane. Let $\phi(z|E)$ denote the Bloch wavefunction deep in the metal and $\phi^*(z|E)$ the time reversed version of $\phi(z|E)$. The eigenfunction in the semi-infinite metal (z<0) has been chosen to have the form as

$$\psi_i(z|E) = \phi(z|E) - P\,\phi^*(z|E) \qquad (4.3)$$

where P is the reflection coefficient which was evaluated by matching the wavefunction and the slope at z=0. We consider the potential V(z) as shown in Fig. (4.1) to be one dimensional

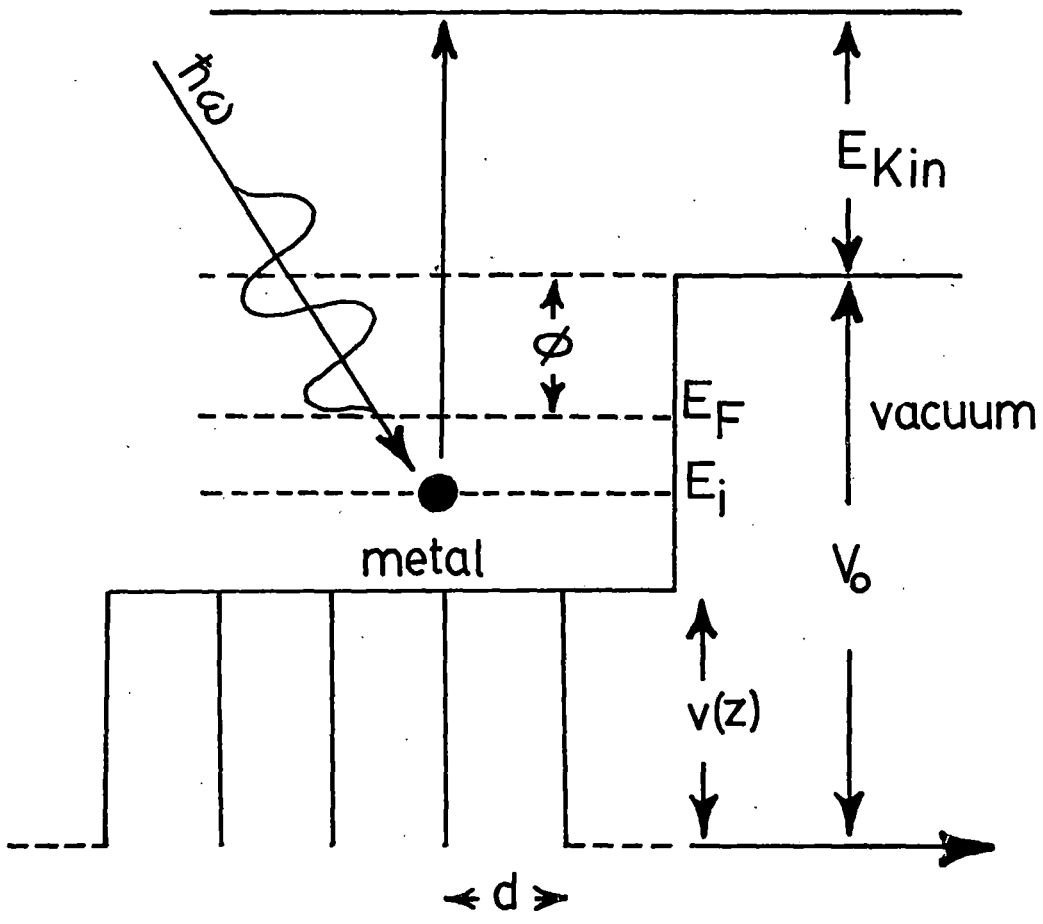

Figure 4.1

Kronig-Penney type described by

$$V(z) = \sum g\, \delta(z - (2n+1)\frac{d}{2}) \tag{4.4}$$

To find $\phi(z|E)$, let us consider an electron with initial state energy $E_i = \hbar^2 k_i^2/2m$ to be incident on the single barrier potential $v(z)$ of width d. Since $v(z)=0$ for $z \geq d/2$, the wavefunction $\phi(z)$ in these regions is described as

$$\phi(z) = \begin{cases} e^{ik_i z} + re^{-ik_i z}, & z \leq -d/2 \\ te^{ik_i z}, & z \geq d/2 \end{cases} \tag{4.5}$$

where r and t are the reflection and transmission coefficients through the potential barrier. For Kronig-Penney model, we have[52]

$$r = ie^{i\delta} \sin\delta$$

$$t = e^{i\delta}\cos\delta \tag{4.6}$$

where δ is the phase shift introduced in the transmitted wave the value of which is given by

$$\cot\delta = -\frac{\hbar k_i^2}{mg} \tag{4.7}$$

In Eq. (4.7), g is the strength of δ-potential which describes the bulk potential. Therefore now, Eq. (4.3) can be written in its final form, with the help of Eqs. (4.5) and (4.6), for the region within the solid ($z<0$) as

$$\psi_i(z|E) = (1-iPe^{-i\delta}\sin\delta)e^{ik_i z} - (P-ie^{i\delta}\sin\delta)e^{-ik_i z} \quad (4.8)$$

The initial state wavefunction outside the metal ($z>0$) is

$$\psi_i(z|E) = Te^{-\varkappa z} \quad (4.9)$$

where T is the transmission coefficient across the boundary plane and

$$\varkappa^2 = \frac{2m}{\hbar^2}(V_o - E_i). \quad (4.10)$$

V_o is the step potential at the surface which an electron encounters while transmitting through the boundary surface. By proper matching $\psi_i(z)$ in Eqs. (4.8) and (4.9) at the surface, we get

$$P = \frac{(\varkappa-ik_i) - (k_i-i\varkappa)e^{i\delta}\sin\delta}{(\varkappa-ik_i) + (k_i-i\varkappa)e^{-i\delta}\sin\delta} \quad (4.11)$$

$$T = \frac{2k_i \sin 2\delta}{(\varkappa - ik_i) + (k_i - i\varkappa)e^{-i\delta}\sin\delta} \qquad (4.12)$$

The proper evaluation of P and T with the appropriate numerical values for other factors enables one to write explicitly the initial state wavefunction ψ_i. The photoemission cross-section was calculated by using the formula

$$\frac{d\sigma}{d\Omega} = \frac{k^2}{\omega} |\langle \psi_f | H' | \psi_i \rangle|^2 \qquad (4.13)$$

The matrix element $I=\langle \psi_f | H' | \psi_i \rangle$ in Eq. (4.13) can be written as

$$I = \int_{-\infty}^{-a/2} \psi_f^* \tilde{A}_\omega(z) \frac{d\psi_i}{dz} dz + \int_{-a/2}^{0} \psi_f^* \tilde{A}_\omega(z) \frac{d\psi_i}{dz} dz$$

$$+\frac{1}{2} \int_{-a/2}^{0} \psi_f^* \frac{d\tilde{A}_\omega(z)}{dz} \psi_i \, dz + \int_{0}^{a/2} \psi_f^* \tilde{A}_\omega(z) \frac{d\psi_i}{dz} dz$$

$$+\frac{1}{2} \int_{0}^{a/2} \psi_f^* \frac{d\tilde{A}_\omega(z)}{dz} \psi_i \, dz + \int_{a/2}^{\infty} \psi_f^* \tilde{A}_\omega(z) \frac{d\psi_i}{dz} dz. \qquad (4.14)$$

The photocurrent was calculated numerically with the help of Eqs. (4.13) and (4.14). The detailed evaluation of the integrals in Eqs. (4.14) is shown in appendix II and the

fortran program in appendix IV. We have used a number of dielectric functions corresponding to different elements. The data for these were those given by Weaver[25] and Edwards[53]. Since it is a model calculations, we have chosen the following data (in atomic units) for all the solids:

$E_i = 0.43$

$\delta = -0.5753$

$g = 0.60$

$\theta_i = 45^o$

The results obtained with using the dielectric function $\varepsilon(\omega)$ for aluminium as given by Weaver[25] are shown in Figs. (4.2) and (4.3). The plots of photocurrent versus the photon energy for the surface region defined by $-a/2 \leq z \leq a/2$ having the surface width a=5 a.u and 10 a.u are shown in Figs. (4.2) and (4.3) respectively. For a=5 a.u, the current peaked at $\hbar\omega$=12 eV then it showed a minimum at $\hbar\omega$=15 eV which is close to the plasmon energy. There is a second peak in the photocurrent data which occurs at around 20 eV and is a broad one. For a=10 a.u (Fig. 4.3), we find a sharp peak at 11 eV and a broad one at 21 eV. The ratio of the two peak heights for a=10 a.u at 11 eV and 21 eV is about 3. These results are in qualitative agreement with the one obtained by using the free electron model[24]. However the peaks below the plasmon energy for the free electron case was much sharper compared to this model.

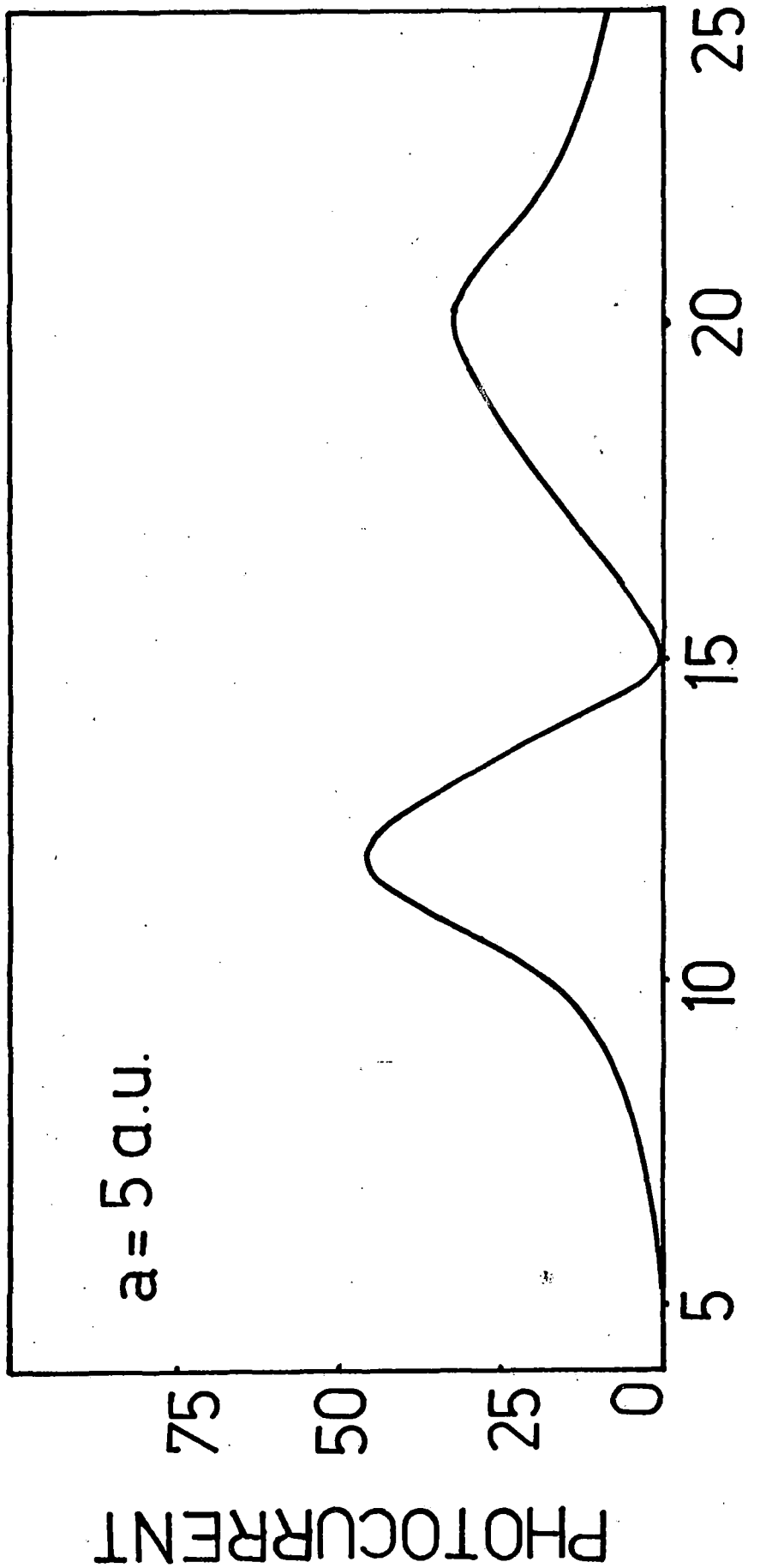

Figure 4.2

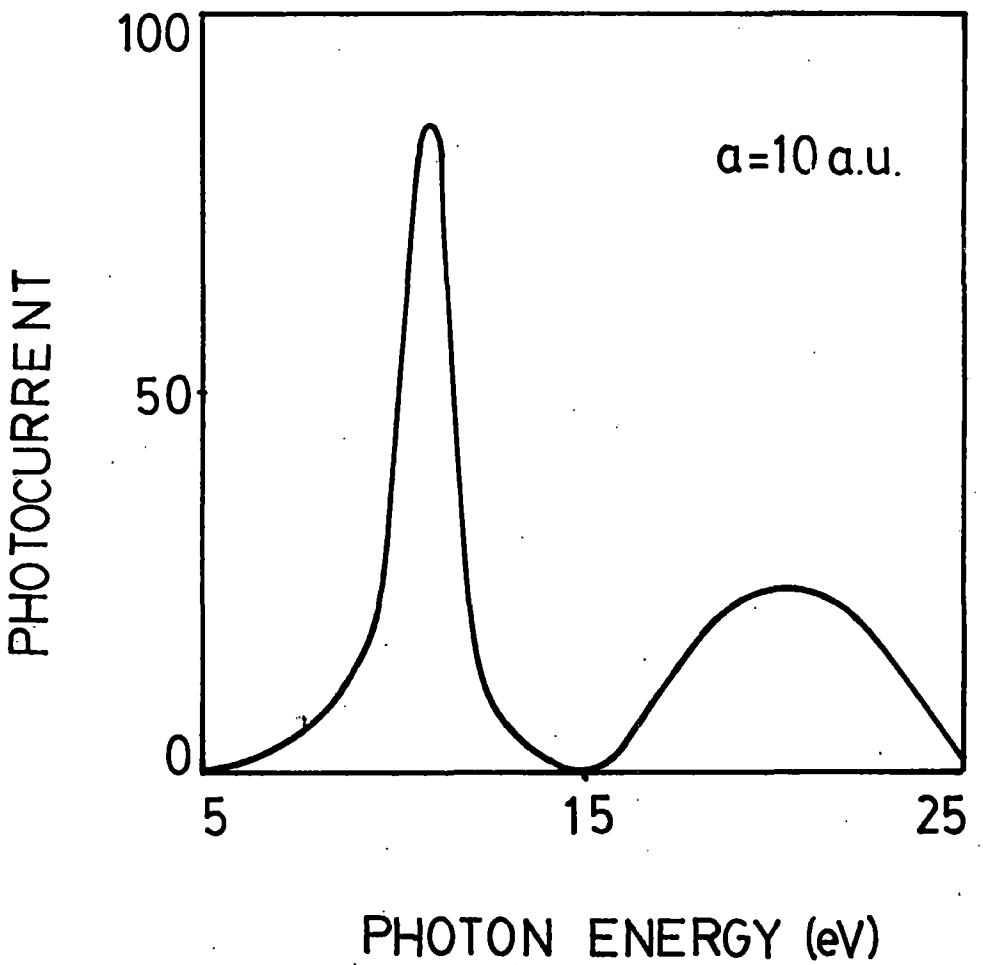

Figure 4.3

Interestingly, the results obtained with α=0.5 and a=10 a.u seem to be in better agreement with the experimental results than the free electron model. Fig. (4.4) shows the photocurrent data for aluminium with no surface region. In this case, there is no minimum at the plasmon energy and the behaviour is qualitatively different from the one obtained with the surface region. This clearly indicates the importance of including the surface region the conclusion which we also reached while doing the free electron model calculations.

We have also used[54] this model with the dielectric function of tungsten. The data used are those of Weaver[25]. We have kept the same Kronig-Penney parameters δ and g as before and we used the same E_i. The results for α=0.5 and a=10 a.u are shown in Fig. (4.5). As expected there is a minimum around the plasmon energy ($\hbar\omega_p$) which in this case is about 25 eV. There is a peak below $\hbar\omega_p$ and another broad one above it. In this respect the behaviour is similar to that obtained with aluminium dielectric functions. We also did a calculation without any surface region (Fig. 4.6) and again we find that the minimum at the plasmon energy is missing, rather there is a maximum at 27 eV. Experimental observations of photocurrent from the tungsten (100) surface state did show a minimum at $\hbar\omega_p$ and this supports our conclusion that the surface variation of the photon field is important in analysing this type of

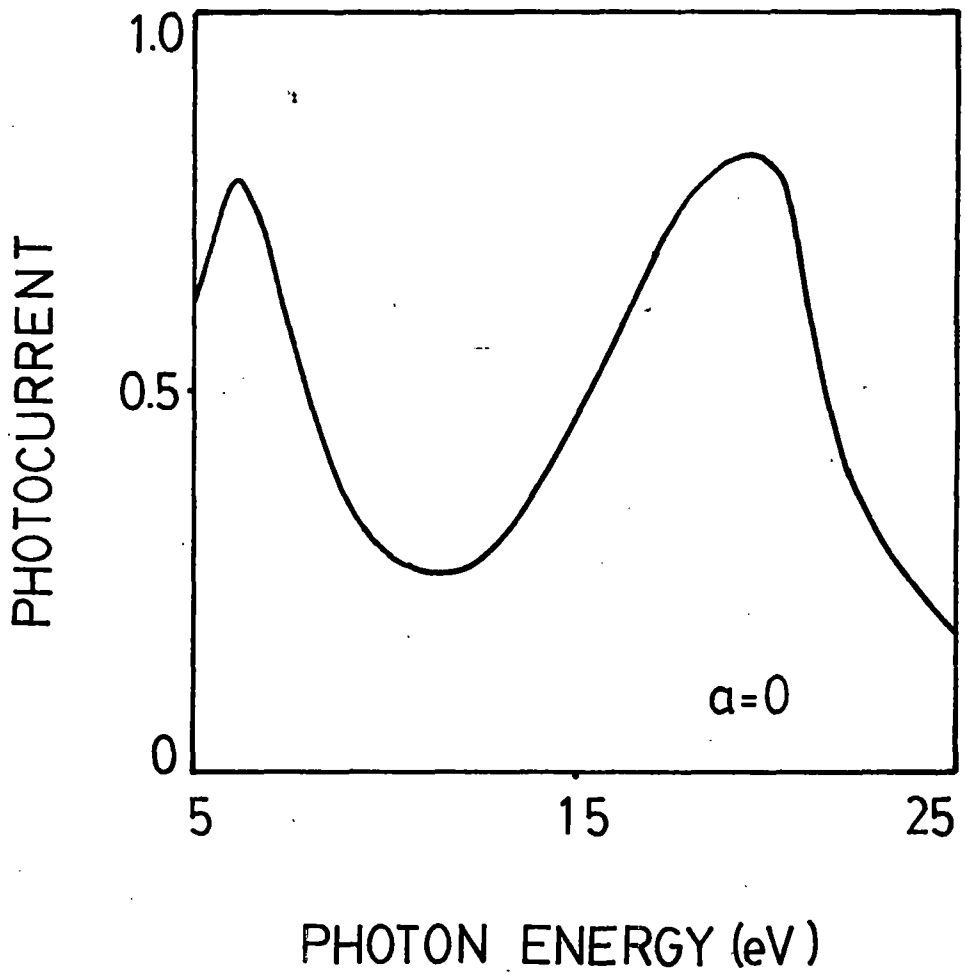

Figure 4.4

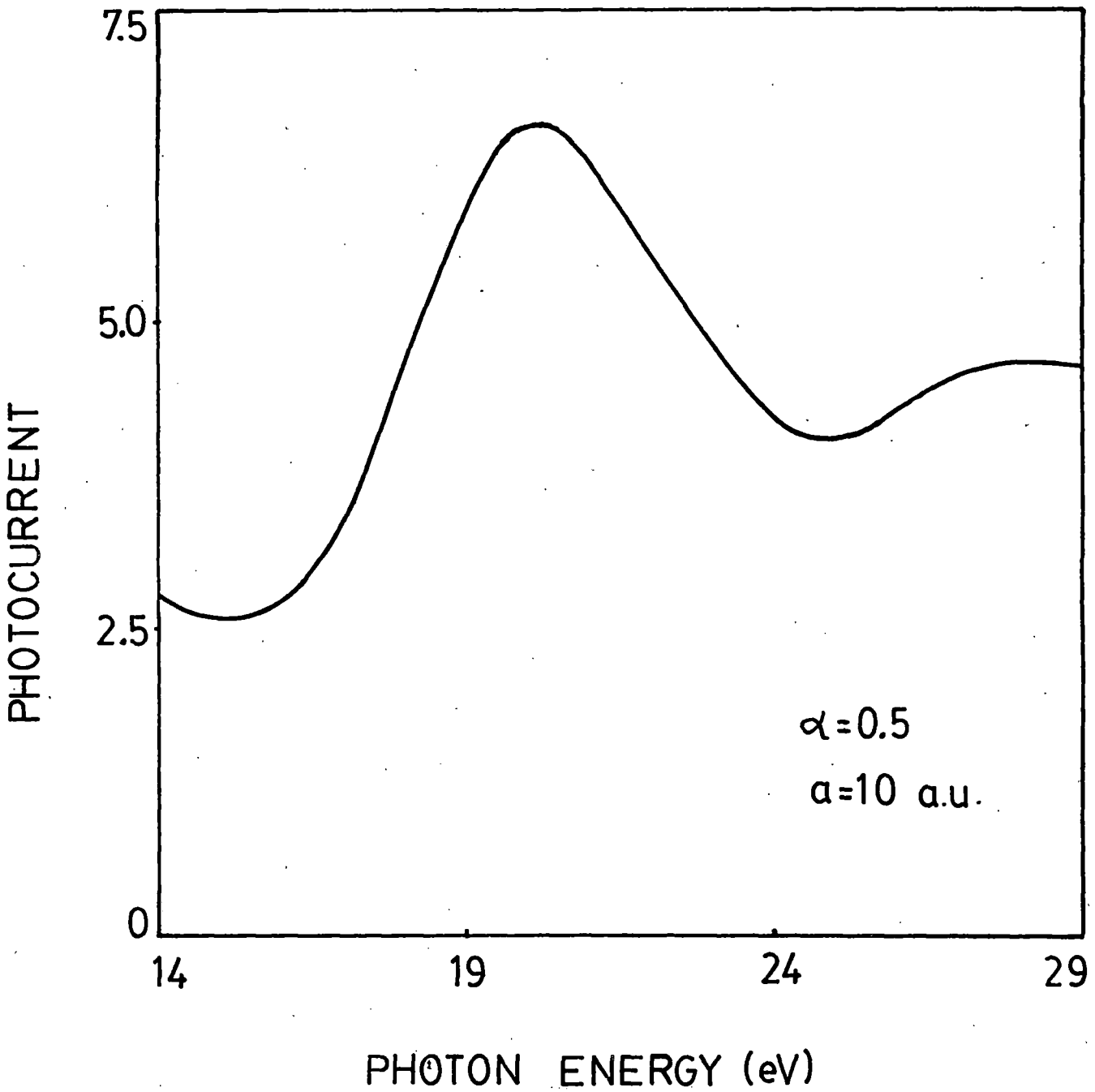

Figure 4.5

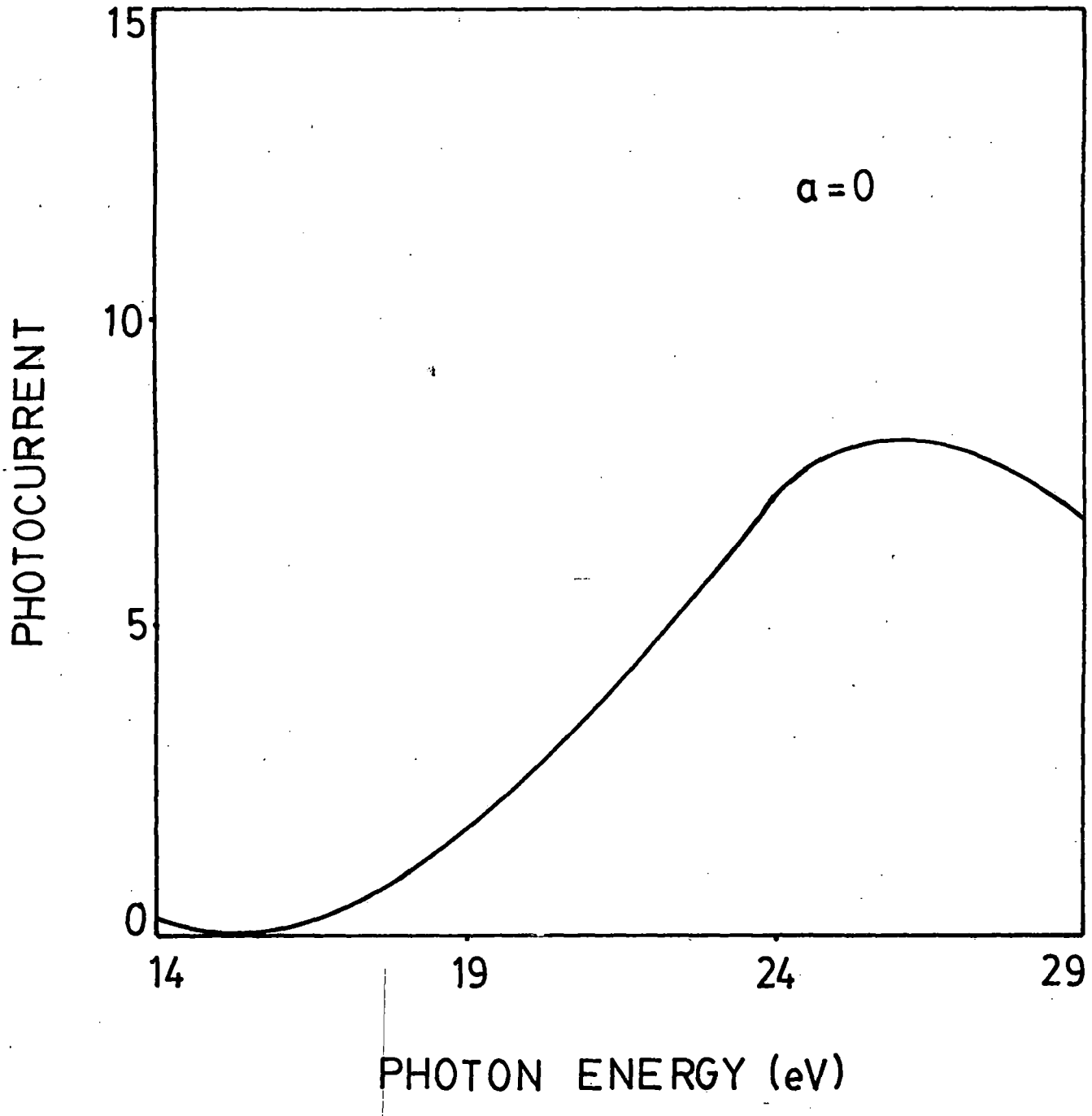

Figure 4.6

spectrum.

We have also used[54] this model in conjunction with the dielectric function $\varepsilon(\omega)$ for silicon as given by Edwards[53] which is a semiconductor and has somewhat different dielectric response. With the same Kronig-Penney parameters and the same E_i, the results for α=0.5 and a=10 a.u are shown in Fig. (4.7). As in other cases, there is a minimum at the plasmon energy around 16 eV. There is maximum below $\hbar\omega_p$ and the currrent rises also beyond $\hbar\omega_p$. But in this case, we see another minimum which is at 21 eV. The reason for this can be traced to the behaviour of $\varepsilon(\omega)$ for silicon which has a resonance in the region of 21 eV. This instability can be seen in Fig. (4.8) for $\varepsilon_1(\omega)$ and $\varepsilon_2(\omega)$ as a function of $\hbar\omega$. As a result of this, the fields inside the solid become vanishingly small (see Fig. 2.13) and consequently the photocurrent also shows a minimum. The photocurrent calculated with no surface region i.e., with Fresnel fields, as shown in (Fig. 4.9) shows no minimum at 16 eV or at 21 eV but it has a maximum at 21 eV. This again shows that the behaviour with and without the surface region is strikingly different.

We next changed the Kronig-Penney parameters g and δ with the new values being g=-0.1070 and δ=0.10, keeping everything else the same to see whether there is any marked change. We find that the behaviour is essentially the same as before which

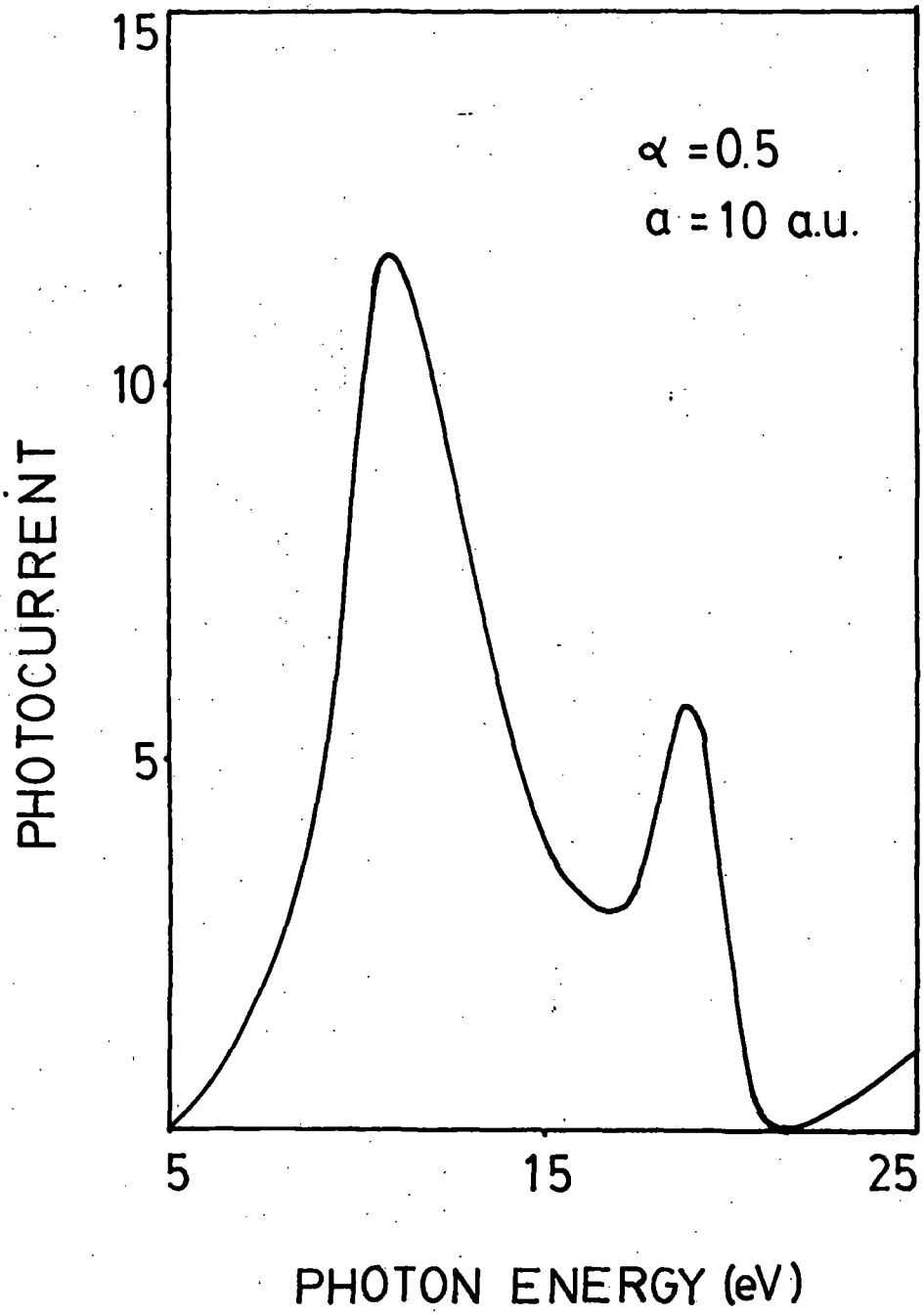

Figure 4.7

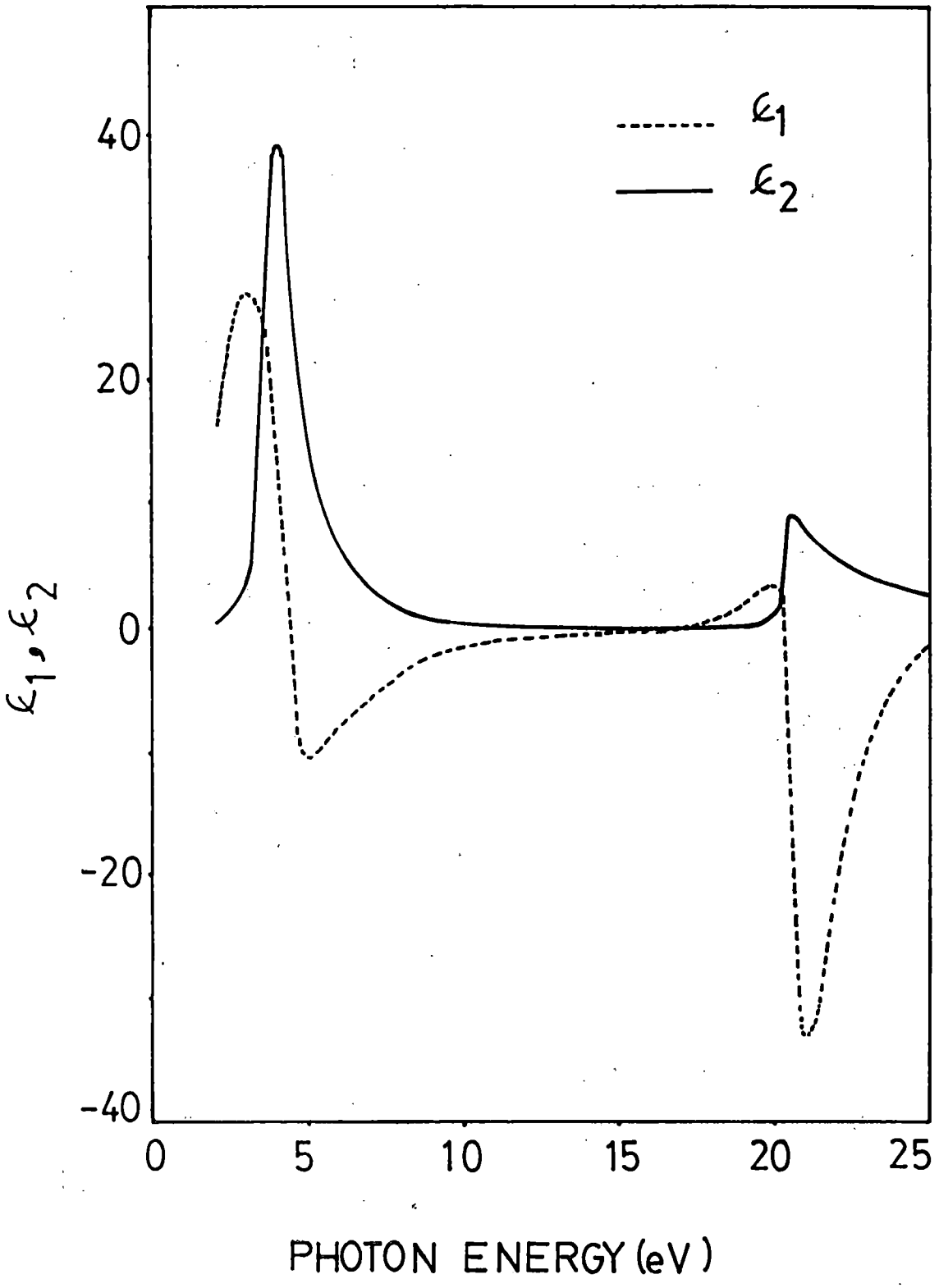

Figure 4.8

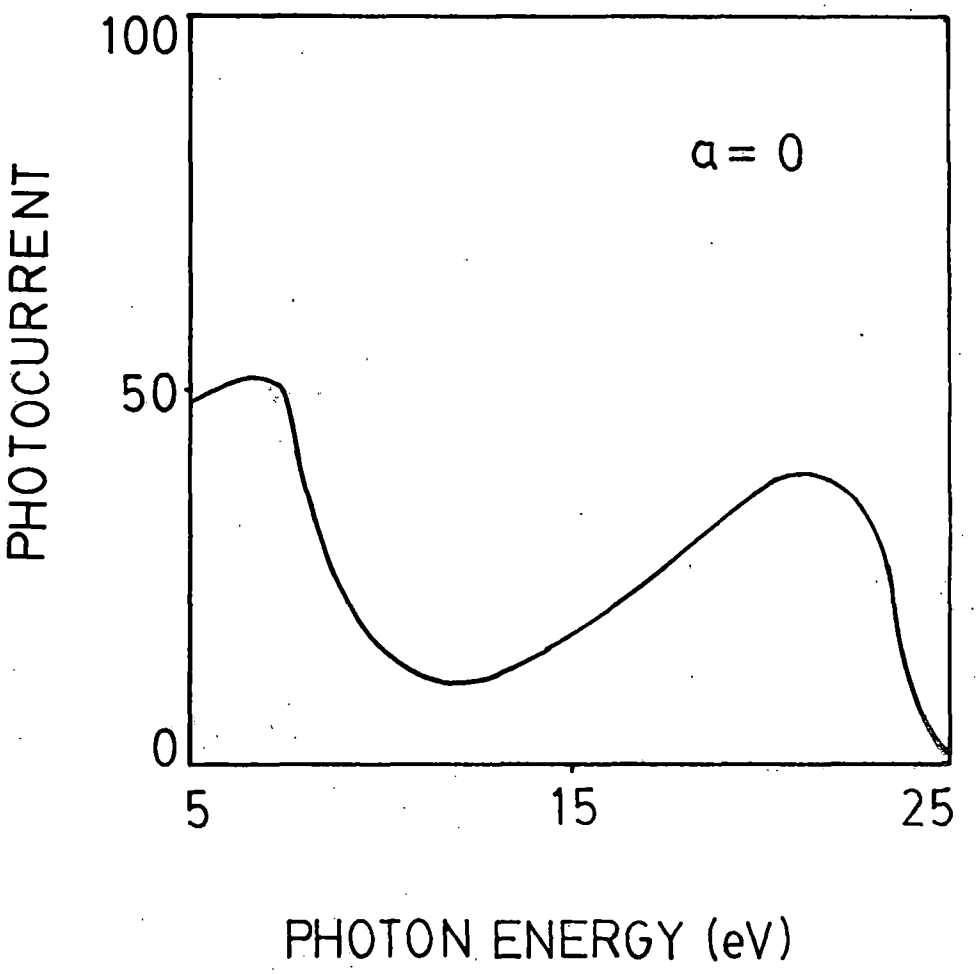

Figure 4.9

is shown in Fig. (4.10).

We have also used this model for calculating the photocurrent using the dielectric function $\varepsilon(\omega)$ of aluminium but with the surface region defined somewhat differently i.e., $-a \leq z \leq 0$ which is shown in Fig. (4.11). The parameters for the Kronig-Pennney model and the value of α and a are the same as used previously for Fig. (4.3) with the same E_i. The matrix element used for the photocurrent cross-section calculation may now be written as

$$I = \langle \psi_f | H' | \psi_i \rangle = \int_{-\infty}^{\infty} \psi_f^*(z) H' \psi_i(z) dz$$

$$= \int_{-\infty}^{-a} \psi_f^* \tilde{A}_\omega(z) \frac{d\psi_i}{dz} dz + \int_{-a}^{0} \psi_f^* \tilde{A}_\omega(z) \frac{d\psi_i}{dz} dz$$

$$+ \frac{1}{2} \int_{-a}^{0} \psi_f^* \frac{d\tilde{A}_\omega(z)}{dz} \psi_i dz + \int_{0}^{\infty} \psi_f^* \tilde{A}_\omega(z) \frac{d\psi_i}{dz} dz$$

There are now four terms as opposed to six terms for the previous case. The photocurrent computed for this case is shown in Fig. (4.12). The photocurrent shows a peak at photon energy 7 eV and a minimum near the plasmon energy of aluminium i.e.,15 eV. There is a second peak in the photocurrent at 20 eV. The ratio between the two peaks at 7 eV and 20 eV is 3 -comparable to the case of the surface region $-a/2 \leq z \leq a/2$. However, we

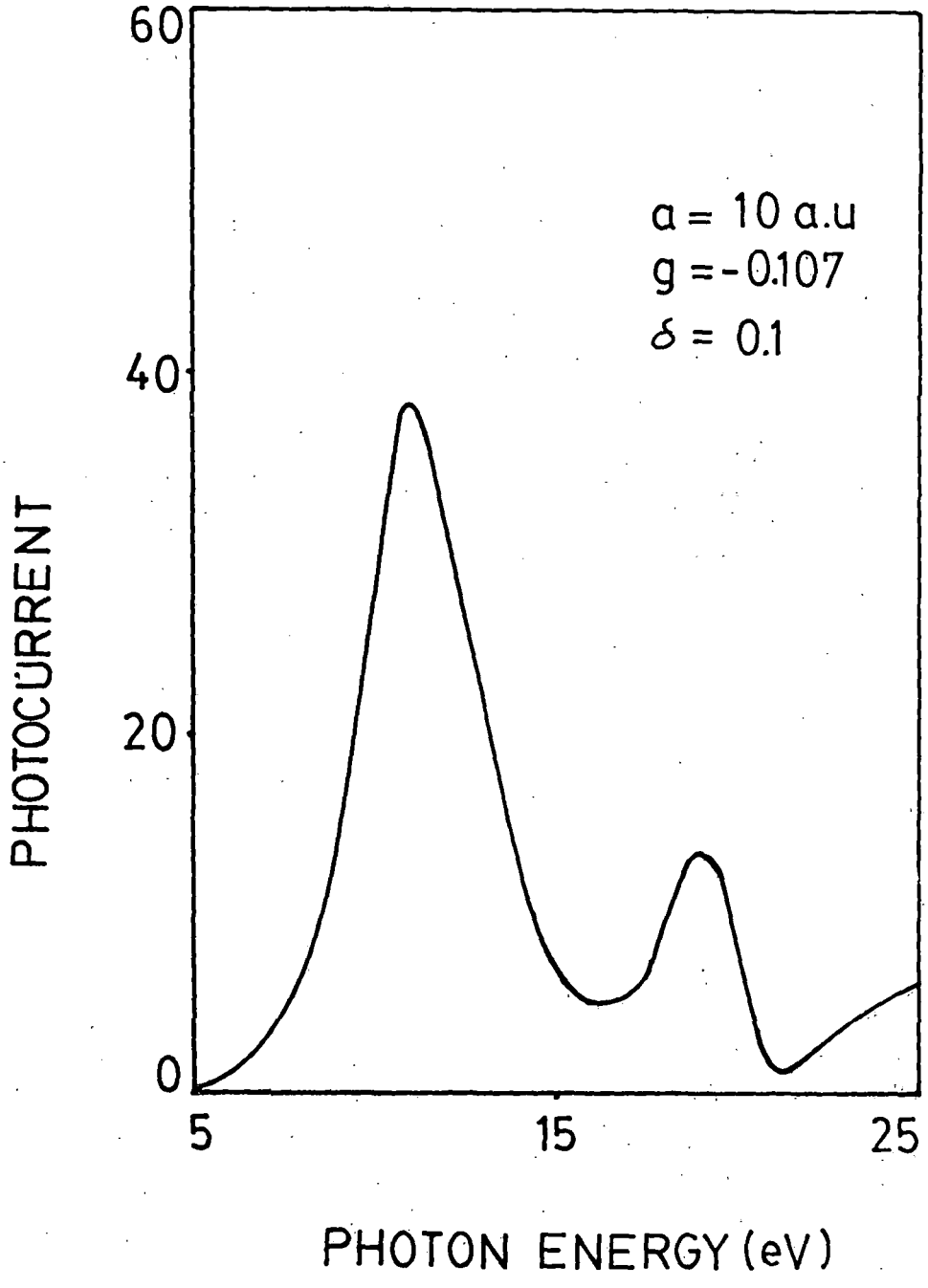
60
40
20
0
5
15
25
a = 10 a.u
g = -0.107
δ = 0.1
PHOTOCURRENT
PHOTON ENERGY (eV)

Figure 4.10

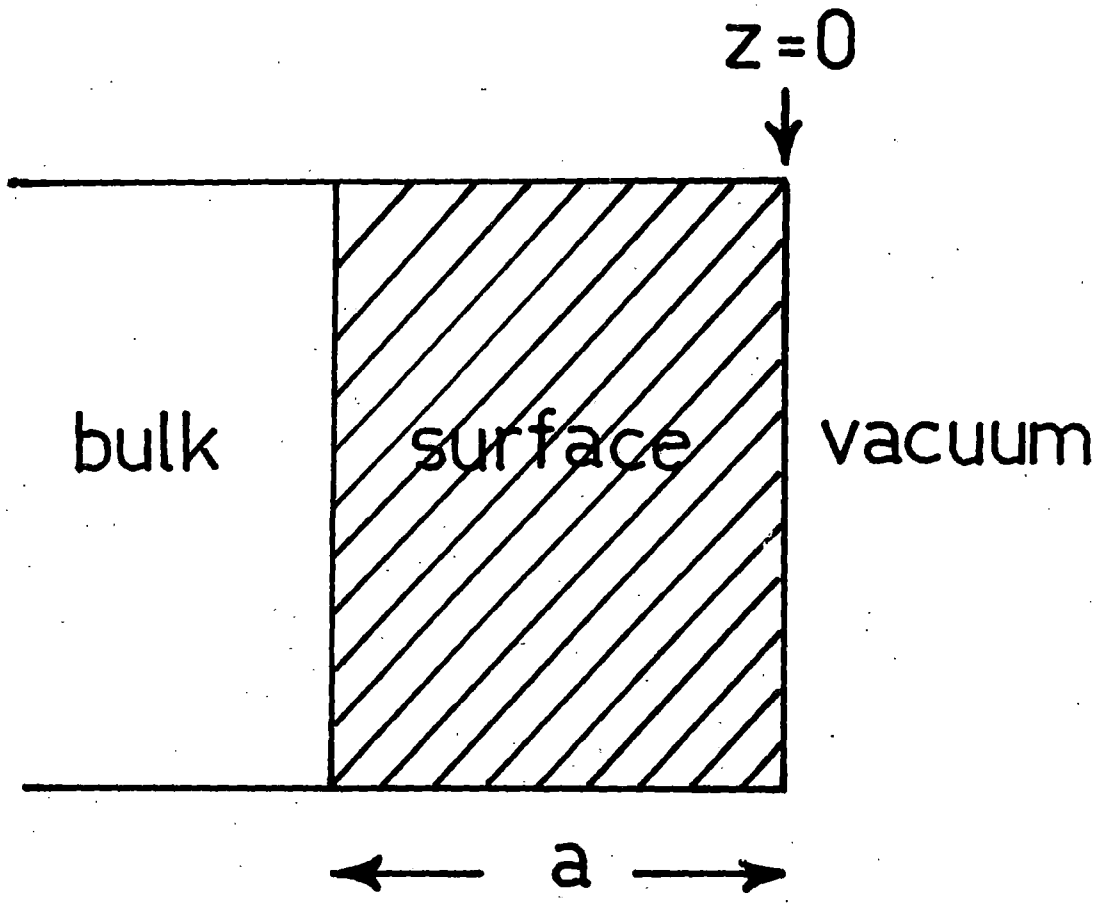

Figure 4.11 -

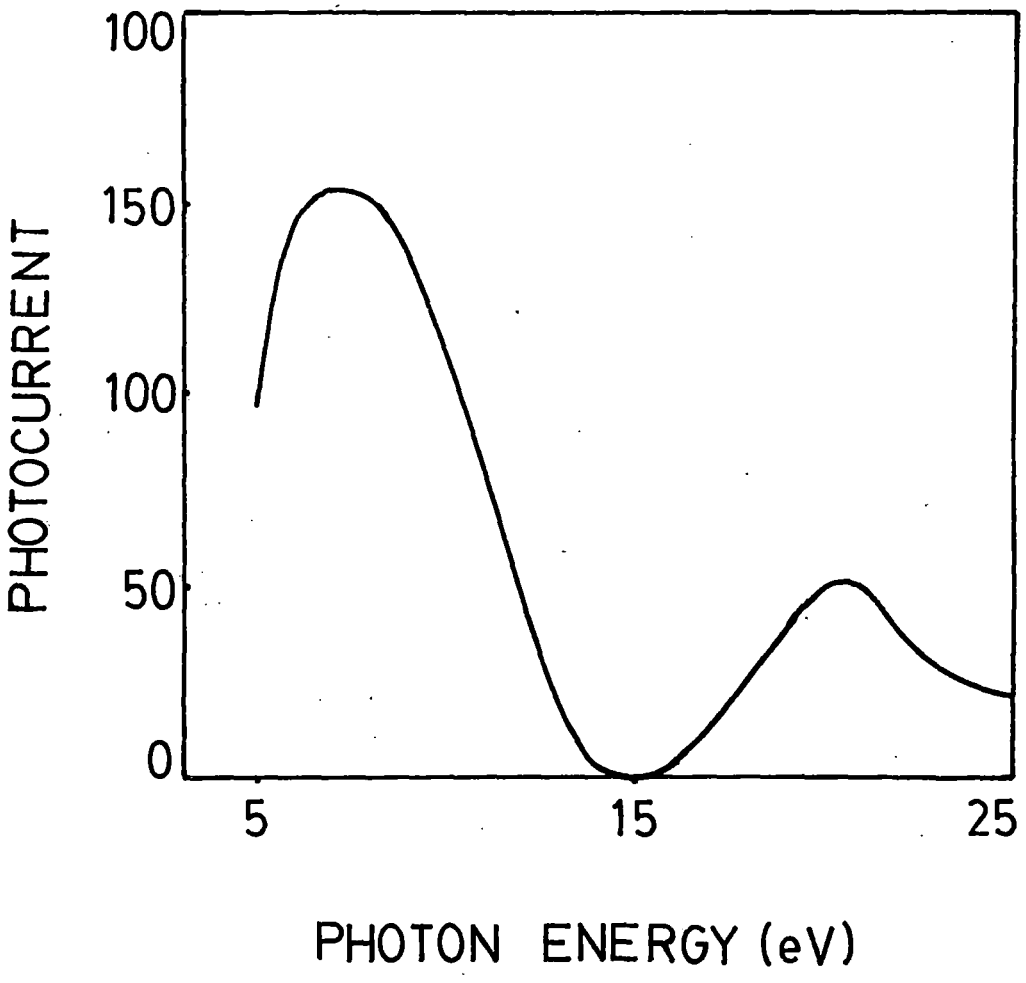

Figure 4.12

see that the peak before $\hbar\omega_p$ shifts in energy and becomes broader. We had calculated the photocurrent in this case also with a sharp surface and no surface region. The results are shown in Fig. (4.13). There is no minimum at the plasmon energy as in all the such cases.

A study of these cases shows that the surface variation of the photon field is important in calculating photoemission cross-section, since neglecting it fails to reproduce the minimum at the plasmon energy. We also see that using dielectric functions corresponding to different elements changes the results. All of these point to the fact that a full fledged photoemission calculation should include the correct variation of photon field near the surface.

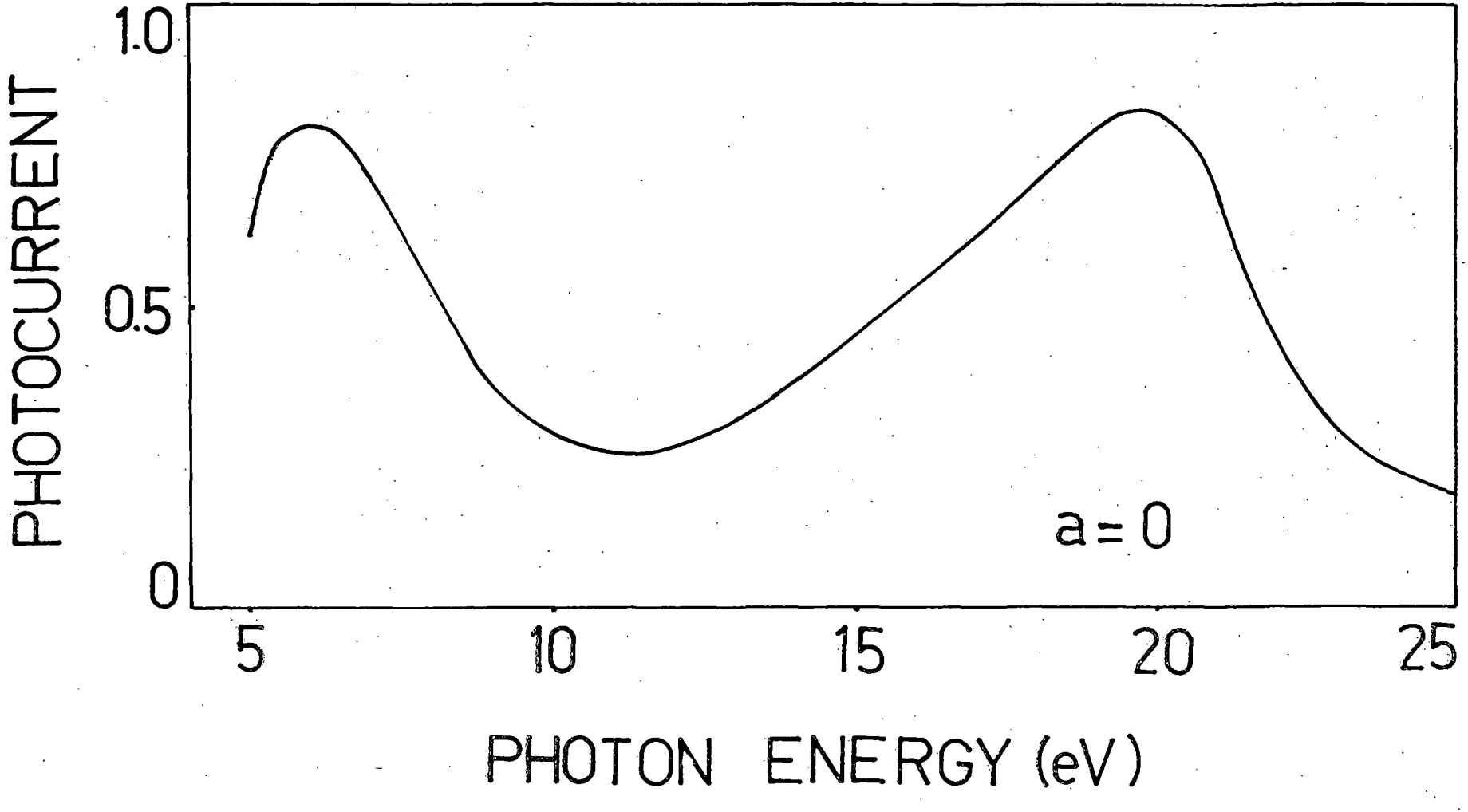

Figure 4.13